Free-energy landscape of mechanically unfolded model proteins: Extended Jarzinsky versus inherent structure reconstruction

Stefano Luccioli,[1,2,*] Alberto Imparato,[3,†] and Alessandro Torcini[1,2,4,‡]
[1]*Istituto dei Sistemi Complessi, CNR, via Madonna del Piano 10, I-50019 Sesto Fiorentino, Italy*
[2]*INFN, Sezione Firenze, and CSDC, via Sansone, 1-I-50019 Sesto Fiorentino, Italy*
[3]*ISI Foundation, Viale Settimio Severo 65, Villa Gualino, I-10133 Torino, Italy*
[4]*Centre de Physique Théorique, Campus de Luminy, 13288 Marseille, France*
(Received 12 March 2008; revised manuscript received 13 August 2008; published 8 September 2008)

The equilibrium free-energy landscape of off-lattice model heteropolymers as a function of an internal coordinate, namely the end-to-end distance, is reconstructed from out-of-equilibrium steered molecular dynamics data. This task is accomplished via two independent methods: By employing an extended version of the Jarzynski equality and the inherent structure formalism. A comparison of the free energies estimated with these two schemes with equilibrium results obtained via the umbrella sampling technique reveals a good quantitative agreement among all the approaches in a range of temperatures around the "folding transition" for the two examined sequences. In particular, for the sequence with good foldability properties, the mechanically induced structural transitions can be related to thermodynamical aspects of folding. Moreover, for the same sequence the knowledge of the landscape profile allows for a good estimation of the lifetimes of the native configuration for temperatures ranging from the folding to the collapse temperature. For the random sequence, mechanical and thermal unfolding appear to follow different paths along the landscape.

DOI: 10.1103/PhysRevE.78.031907 PACS number(s): 87.15.A−, 82.37.Rs, 05.90.+m, 87.15.Cc

I. INTRODUCTION

Several states of matter are characterized by a nontrivial free-energy landscape (FEL), which can be at the origin of peculiar structural and dynamical features. Supercooled liquids, glasses, atomic clusters, and biomolecules [1] are typical examples of systems whose thermodynamical behavior can be traced back to the intricate topological properties of the underlying FEL. The pioneering work by Stillinger and Weber on inherent structures (ISs) of liquids [2] revealed the importance of investigating the stationary points of the potential energy surface (PES) for characterizing their dynamical and thermodynamical properties. Similar approaches have been proposed and successfully applied, in glasses [3] and supercooled liquids [4], to the identification of the structural-arrest temperature. This temperature marks a topological transition from a dynamics evolving in a landscape dominated by minima to one where unstable saddles play a major role [4,5].

More recently, this kind of analysis has been applied to the study of protein models [1,6–12]. In particular, several studies have been devoted to the reconstruction of the PES and of the FEL topology in terms of graphs (at various levels of coarse graining) connecting the folded states to the unfolded structures [7–9]. The knowledge of the graph structure connecting the various metastable states and of the probability transitions among them allows for a reconstruction of the folding dynamics in terms of a master equation [13]. Moreover, detailed analysis of the thermodynamical and dynamical features, characteristics of proteins, have been quite recently carried out in terms of ISs [10–12]. These analysis suggest that the folding process of a protein towards its native configuration depends crucially on the structure and topological properties of its (free-) energy landscape. Confirming somehow the conjecture that the FEL of a protein has a funnel-like shape: The native configuration being located inside the so-called native valley at the bottom of the funnel itself [14].

On the other hand, mechanical unfolding of single biomolecules represents a powerful technique to extract information on their internal structure as well as on their unfolding and refolding pathways [15–19]. However, mechanical unfolding of biomolecules is an out-of-equilibrium process: Unfolding events occur on time scales much shorter than the typical relaxation time of the molecule towards equilibrium. Nonetheless, by using the equality introduced by Jarzynski [20], the free energy of mechanically manipulated biomolecules can be recovered as a function of an externally controlled parameter [21,22]. Moreover, an extended version of the Jarzynski equality (EJE) has been proposed in order to estimate the equilibrium free-energy landscape in absence of applied forces as a function of an internal coordinate of the system (usually, the end-to-end distance ζ) [23–26]. Quite recently this approach has been successfully applied to data obtained from nanomanipulation of titin I27 domain with atomic force microscopy (AFM) [27,28] and from steered molecular dynamics simulations of a mesoscopic off-lattice protein model [29]. The analysis reported in [29] was devoted to a single sequence previously identified as a reasonably fast folder [30,31] and it was essentially performed at a unique temperature.

As an extension of the analysis performed in Ref. [29], in the present paper we reconstruct, for two different sequences with bad and good folding properties, the equilibrium FEL as

*stefano.luccioli@fi.isc.cnr.it
†Present address: Department of Physics and Astronomy, University of Aarhus, Denmark. alberto.imparato@polito.it
‡alessandro.torcini@cnr.it

a function of the end-to-end distance ζ in two distinct ways: Namely, by employing the EJE approach and the IS distributions. We will show that specific features of the landscapes characteristic of a protein, i.e., a good folder, can be singled out from a comparison of the two approaches. Furthermore, the different unfolding structural transitions can be associated to the detachment of specific strands of the examined heteropolymers. In particular, the investigation of the IS distributions allows us to give an estimate of the energetic and entropic barriers separating the native state from the completely stretched configuration. Moreover, for the good folder the temperature dependence of the free-energy barrier heights and the unfolding times can be related.

An important aspect to clarify is the relationship between the thermal and mechanical unfolding pathways of proteins: Experimental [32] as well as numerical works [33,34] seem to suggest that these paths are indeed different. However, there are indications that the thermal paths can be recovered also via the manipulation procedure in the limit of very low pulling velocities [34]. This seems to be in agreement with our findings for the good folder, which indicate that the observed structural transitions, induced by mechanical unfolding, can be put in direct relationship with the thermal transitions usually identified for the folding-unfolding process.

The paper is organized as follows, Sec. II is devoted to the introduction of the employed model and sequences, as well as of the simulation protocols. In Sec. III it is explained how to combine the umbrella sampling technique [35] with the weighted histogram analysis method [36] in order to recover the equilibrium free-energy profile as a function of an internal coordinate of the system. The inherent structure formalism and the extended Jarzynski equality are briefly illustrated in Sec. IV and Sec. V, respectively. The thermodynamical properties of the studied sequences are reported in Sec. VI. While Sec. VII (respectively, Sec. VIII) is devoted to the free-energy landscape reconstruction in terms of the extended Jarzinsky equality (respectively, inherent structure approach). In Sec. VIII the two methods are also compared and discussed. Finally, the results are summarized in Sec. IX.

II. MODEL AND SIMULATION PROTOCOL

A. Model

The model studied in this paper is a modified version of the three-dimensional (3D) off-lattice model introduced by Honeycutt-Thirumalai [37] and successively generalized by Berry *et al.* to include a harmonic interaction between next-neighboring beads instead of rigid bonds [38]. This model has been widely studied in the context of thermally driven folding and unfolding [9,11,30,31,37–40] and only more recently for what concerns mechanical folding and refolding [41,42]. The model consists of a chain of L pointlike monomers mimicking the residues of a polypeptidic chain. For the sake of simplicity, only three types of residues are considered: Hydrophobic (B), polar (P), and neutral (N) ones.

The intramolecular potential is composed of four terms: A stiff nearest-neighbor harmonic potential, V_1, intended to maintain the bond distance almost constant, a three-body interaction V_2, which accounts for the energy associated to bond angles, a four-body interaction V_3 corresponding to the dihedral angle potential, and a long-range Lennard-Jones (LJ) interaction, V_4, acting on all pairs i, j such that $|i-j|>2$, namely

$$V_1(r_{i,i+1}) = \alpha(r_{i,i+1} - r_0)^2, \tag{1}$$

$$V_2(\theta_i) = A\cos(\theta_i) + B\cos(2\theta_i) - V_0, \tag{2}$$

$$V_3(\varphi_i, \theta_i, \theta_{i+1}) = C_i[1 - S(\theta_i)S(\theta_{i+1})\cos(\varphi_i)] + D_i[1 - S(\theta_i)S(\theta_{i+1})\cos(3\varphi_i)], \tag{3}$$

$$V_4(r_{i,j}) = \varepsilon_{i,j}\left(\frac{1}{r_{i,j}^{12}} - \frac{c_{i,j}}{r_{i,j}^{6}}\right). \tag{4}$$

Here, $r_{i,j}$ is the distance between the ith and the jth monomer, θ_i and φ_i are the bond and dihedral angles at the ith monomer, respectively. The parameters $\alpha=50$ and $r_0=1$ (both expressed in adimensional units) fix the strength of the harmonic force and the equilibrium distance between subsequent monomers (which, in real proteins, is of the order of a few Å). The value of α is chosen to ensure a value for V_1 much larger than the other terms of potential in order to reproduce the stiffness of the protein backbone. The expression for the bond-angle potential term $V_2(\theta_i)$ (2) corresponds, up to the second order, to a harmonic interaction term $\sim(\theta_i-\theta_0)^2/2$, where

$$A = -k_\theta\frac{\cos(\theta_0)}{\sin^2(\theta_0)}, \quad B = \frac{k_\theta}{4\sin^2(\theta_0)},$$

$$V_0 = A\cos(\theta_0) + B\cos(2\theta_0), \tag{5}$$

with $k_\theta=20\epsilon_h$, $\theta_0=5\pi/12$ rad or 75° and where ϵ_h sets the energy scale. This formulation in terms of cosines allows us to speed up the simulation, since it is sufficient to evaluate $\cos(\theta_i)$ and the value of bond angle is not needed, and at the same time to avoid spurious divergences in the force expression due to the vanishing of $\sin(\theta_i)$ when three consecutive atoms become aligned [43].

The dihedral angle potential is characterized by three minima for $\varphi=0$ (associated to a so-called *trans* state) and $\varphi=\pm 2\pi/3$ (corresponding to gauche states), this potential is mainly responsible for the formation of secondary structures. In particular, large values of the parameters C_i, D_i favor the formation of trans state and therefore of β sheets, while when gauche states prevail α helices are formed. The parameters (C_i, D_i) have been chosen as in [39], i.e., if two or more beads among the four defining φ are neutral (N) then $C_i=0$ and $D_i=0.2\varepsilon_h$, in all the other cases $C_i=D_i=1.2\varepsilon_h$ (see Fig. 1). The tapering function $S(\theta_i)=1-\cos^{32}(\theta_i)$ has been introduced in the expression of V_3 in order to cure a well-known problem in the dihedral potentials [43]. This problem is encountered whenever $\theta_i=0$ or π, i.e., when three consecutive beads are in the same line, in these situations the associated dihedral angle is no more defined and a discontinuity in V_3 arises. In contrast to what was reported in [43] this situation is not improbable for the present model. The quantity $S(\theta_i)S(\theta_{i+1})$ entering in the definition of V_3 has a limited

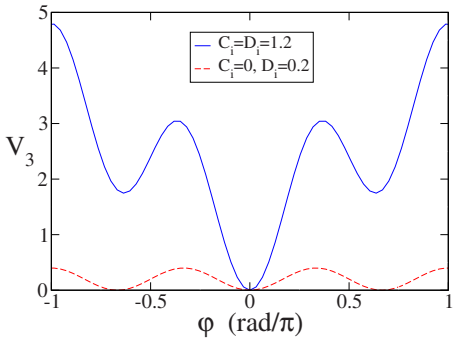

FIG. 1. (Color online) Dihedral angle potential, V_3, when two or more beads among the four defining φ are neutral (red dashed curve), and in all of the other cases (blue solid curve). We fixed $\varepsilon_h=1$ and $S(\theta_i)=S(\theta_{i+1})\equiv 0$.

influence on the dynamics apart in proximity of the above-mentioned extreme cases. Moreover, $S(\theta_i)S(\theta_{i+1})$ is C^∞, its value is essentially 1 almost for any θ_i, it does not introduce any extra minima in the potential and it vanishes smoothly for $\theta_i \to 0$ or $\theta_i \to \pi$ [44].

The last term V_4 has been introduced to mimic effectively the interactions with the solvent, it is a Lennard-Jones potential and it depends on the type of interacting residues as follows:

(i) If any of the two monomers is neutral the potential is repulsive $c_{N,X}=0$ and its scale of energy is fixed by $\varepsilon_{N,X}=4\varepsilon_h$.

(ii) For interactions between hydrophobic residues $c_{B,B}=1$ and $\varepsilon_{B,B}=4\varepsilon_h$.

(iii) For any polar-polar or polar-hydrophobic interaction $c_{P,P}\equiv c_{P,B}=-1$ and $\varepsilon_{P,P}\equiv\varepsilon_{P,B}=(8/3)\varepsilon_h$.

Accordingly, the Hamiltonian of the system reads as

$$H = K + V = \sum_{i=1}^{L} \frac{p_{x,i}^2 + p_{y,i}^2 + p_{z,i}^2}{2} + \sum_{i=1}^{L-1} V_1(r_{i,i+1}) + \sum_{i=2}^{L-1} V_2(\theta_i) + \sum_{i=2}^{L-2} V_3(\varphi_i, \theta_i, \theta_{i+1}) + \sum_{i=1}^{L-3} \sum_{j=i+3}^{L} V_4(r_{ij}), \tag{6}$$

where, for the sake of simplicity, all monomers are assumed to have the same unitary mass, the momenta are defined as $(p_{x,i}, p_{y,i}, p_{z,i}) \equiv (\dot{x}_i, \dot{y}_i, \dot{z}_i)$ and we fix $\varepsilon_h=1$.

In the present paper we consider the two following sequences of 46 monomers:

(i) $[GF]=B_9N_3(PB)_4N_3B_9N_3(PB)_5P$, a sequence that has been widely analyzed in the past for spontaneous folding [9,11,30,31,37–40] as well as for mechanical unfolding and refolding [41,42].

(ii) $$[BF] = BNBPB_3NPB_4NBPB_2NP_2B_5N_2BPBNPB_2NBP_2BNB_2PB_2,$$

a randomly generated sequence, but with the same number of B, P, and N monomers as the GF.

These two sequences have been chosen because GF has been previously identified as a reasonably fast folder [30] (see also [38] for a detailed and critical analysis of the basin-bottom structures observed for this model), while we expect that the sequence BF, being randomly chosen, cannot have the characteristic of a good folder. From now on we refer to the sequence GF (respectively, BF) as the good (respectively, bad) folder.

The 46-mer sequence GF exhibits a four stranded β-barrel native configuration (NC) with an associated potential energy $E_{\mathrm{NC}}=-49.878$. Please note that the model is here analyzed by employing the same potential and parameter set reported in Ref. [39], but neglecting any diversity among the hydrophobic residues. The NC, displayed in Fig. 6(a), is stabilized by the attractive hydrophobic interactions among the B residues, in particular the first and third B_9 strands, forming the core of the NC, are parallel to each other and antiparallel to the second and fourth strand, namely, $(PB)_4$ and $(PB)_5P$. The latter strands are exposed towards the exterior due to the presence of polar residues.

As shown in Fig. 10, the native structure of the BF is quite different, it has a core constituted by the first three β strands and a very long "tail" (made of 18 residues) wrapped around the core. In particular, the first and second β strands (namely, $BNBPB_3NP$ and B_4NBPB_2) are formed by nine residues, and antiparallel to each other. For more clarity, we will term π_1 as the plane containing the first two strands. The third strand (namely, P_2B_5) is made of seven residues and it is located in a plane lying in-between the first and second strand, which is almost perpendicular to π_1. The chain rotates by almost 90° in correspondence of the two consecutive neutral beads and then exhibits a short strand of three beads PBP before turning back with a parallel strand of seven beads (PB_2NBP_2) that passes below π_1. Finally the chain turns once more back by passing this time above the plane π_1. In the final part of the tail of the chain a short strand of five residues, parallel to the fourth and fifth strands, can be identified as B_2PB_2. The potential energy of the NC of the BF is quite high with respect to the GF, namely, $V_{\mathrm{NC}}=-23.956$. Moreover, this difference, as reported in Table I, is essentially due to the difference in the dihedral contributions, that is much higher in the NC of the BF with respect to the GF, while all of the other contributions, in particular the LJ ones, have nearby values. The dihedral contribution that arises in the BF is essentially due to the configuration of the first three strands, since these are arranged over two almost orthogonal planes.

TABLE I. Potential energy values associated to the NC of the *GF* and *BF*, the different contributions to the total potential energy V_{NC} are also reported.

	GF	*BF*
V_{NC}	−49.878	−23.956
V_1	0.787	0.777
V_2	1.767	5.744
V_3	2.602	23.105
V_4	−55.035	−53.582

B. Simulation protocol: Equilibrium Langevin dynamics

Molecular dynamics (MD) canonical simulations at equilibrium temperature T have been performed by integrating the corresponding Langevin equation for each monomer of unitary mass (characterized by the position vector $\mathbf{r}_i$),

$$\ddot{\mathbf{r}}_i = \mathbf{F}(\mathbf{r}_i) - \gamma\dot{\mathbf{r}}_i + \eta(t), \quad i = 1, L, \tag{7}$$

where $\eta(t)$ is a zero average Gaussian noise term with correlations given by $\langle \eta_\alpha(t)\eta_\beta(t')\rangle = 2T\gamma\delta(t-t')\delta_{\alpha,\beta}$; $\mathbf{F} = -\nabla V$, being V the intramolecular potential introduced in Sec. II A, γ the friction coefficient associated to the solvent and by assuming a unitary Boltzmann constant.

Numerical integrations have been implemented via a standard Euler scheme with a time step $\Delta t = 0.005$ and with a low friction coefficient $\gamma = 0.05$ [39]. Two different kinds of MD have been performed, namely unfolding simulations (US) and folding simulations (FS). In the first case the initial state of the system is taken equal to the native configuration (NC), that we assume to coincide with the minimal energy configuration. In the latter one the initial state is a completely unfolded configuration.

C. Simulation protocol: Out-of-equilibrium mechanical unfolding

In order to mimic the mechanical pulling of the protein attached to a AFM cantilever, or analogously when trapped in an optical tweezer, one extremum of the chain was kept fixed and the last bead is attached to a pulling apparatus with a spring of elastic constant k. The external force is applied by moving the "cantilever" along a fixed direction with a certain protocol $z(t)$. Before pulling the protein, the coordinate system is always rigidly rotated, in order to have the z axis aligned along the end-to-end direction connecting the first and last bead. Therefore, by denoting with ζ the end-to-end distance, the component of the external force along this direction reads as

$$F_{\text{ext}} = k(z - \zeta), \tag{8}$$

where $k = 10$ in order to suppress fast oscillations. As recently pointed out it is extremely important to use a sample of thermally equilibrated initial configurations to correctly reproduce the equilibrium FEL via the JE. [22]. Therefore, before pulling the protein, we have performed a thermalization procedure in two steps. At a fixed temperature T, initially the protein evolves freely starting from the NC for a time $t = 1000$, then it is attached to the external apparatus, with the first bead blocked, and it equilibrates for a further time period $t = 500$. The system (at sufficiently low temperatures) quickly settles down to a "nativelike" configuration. This configuration is then employed as the starting state for the forced folding. The protocol that we have used is a linear pulling protocol with a constant speed v_p, i.e., $z(t) = z(0) + v_p \times t$, by assuming that the pulling starts at $t = 0$. Usually we have employed velocities $v_P \in [5 \times 10^{-6} : 5 \times 10^{-2}]$ and set $z(0) = \zeta_0$, i.e., to the end-to-end distance associated to the native configuration.

III. WEIGHTED HISTOGRAM ANALYSIS METHOD

A combination of the umbrella sampling technique [35] with the weighted histogram analysis method (WHAM) [36] allows us to obtain the equilibrium free-energy profile as a function of the end-to-end distance.

The umbrella sampling technique [35] amounts to perform a series of biased molecular dynamics simulations of the system constrained by an external potential, namely

$$w_i(\zeta) = \tfrac{1}{2}k_W(\zeta - \bar{\zeta}_i)^2. \tag{9}$$

The potential w_i forces the heteropolymer to stay in configurations characterized by a certain average end-to-end distance $\bar{\zeta}_i$, even if at the considered temperature such ζ value is highly unfavored. These simulations allow us to obtain a series of M biased end-to-end probability density distributions $\rho_i^B(\zeta)\{i = 1, \ldots, M\}$, which properly combined can permit the reconstruction of the equilibrium unbiased $\rho(\zeta)$. In particular, in the case of identical statistics for each biased run the WHAM formalism prescribes the following combination:

$$\rho(\zeta) = \frac{\sum_{i=1}^{M} \rho_i^B(\zeta)}{\sum_{i=1}^{M} e^{-\beta[w_i(\zeta) - F_i]}} = e^{-\beta f_W(\zeta,T)}, \tag{10}$$

where $\beta = 1/T$ and the free-energy constants $\{F_i\}$ can be obtained by the normalization condition

$$e^{-\beta F_i} = \int d\zeta e^{-\beta w_i(\zeta)}\rho(\zeta). \tag{11}$$

Equations (10) and (11) should be solved self-consistently via an iterative procedure, finally this allows us to obtain an estimate of the equilibrium free energy $f_W(\zeta, T)$, apart from an additive constant.

We have considered equally spaced $\{\bar{\zeta}_i\}$ values, with a separation $\Delta\bar{\zeta}_i = 0.2$ among them, ranging from the native configuration ζ_0 to the all *trans*-configuration ζ_{trans}.[1]

[1]This is an elongated (planar) equilibrium conformation of the protein with all the dihedral angles at their *trans* values, corresponding to $\zeta_{trans} = 35.70$.

For each of the M runs, after a quite long equilibration time $t \sim 120\,000-200\,000$, we have estimated $\rho_i^B(\zeta)$ over 100 000 configurations taken at regular time intervals $\Delta t=0.2$. The biased simulations have been performed with a hard and weak spring, corresponding to $k_W=10$ and 0.5 in (9), respectively. The results obtained essentially agree for the two k_W values, apart when the free-energy landscape exhibits steep increases as a function of ζ. In these cases the hard spring is more appropriate, since the weak one allows the protein to refold, thus rendering the ζ intervals, where $f_W(\zeta)$ is steeper, not accessible to the WHAM reconstruction.

IV. INHERENT STRUCTURE FORMALISM

Inherent structures correspond to local minima of the potential energy, in particular the phase space visited by the protein during its dynamical evolution can be decomposed into a set of disjoint attraction basins, each corresponding to a specific IS. Therefore, the canonical partition function can be expressed within the IS formalism as a sum over the nonoverlapping basins of attraction, each corresponding to a specific minimum (IS) a [1,10],

$$Z_{\mathrm{IS}}(T) = \frac{1}{\lambda^{3N'}} \sum_a e^{-\beta V_a} \int_{\Gamma_a} e^{-\beta \Delta V_a(\Gamma)} d\Gamma = \sum_a e^{-\beta [V_a + R_a(T)]}, \tag{12}$$

where N' is the number of degrees of freedom of the system, λ is the thermal wavelength, Γ represents one of the possible conformations of the protein within the basin of attraction of a, V_a is the potential energy associated to the minimum a, $\Delta V_a(\Gamma)=V(\Gamma)-V_a$ and $R_a(T)$ the vibrational free energy due to the fluctuations around the minimum.

The vibrational term $R_a(T)$ can be estimated by assuming a harmonic basin of attraction,

$$e^{-\beta R_a(T)} = \frac{1}{\lambda^{3N-6}} \int_{\Gamma_a} e^{-\beta \Delta V_a(\Gamma)} d\Gamma = \prod_{j=1}^{3N-6} \frac{T}{\omega_a^j}, \tag{13}$$

where ω_a^j are the frequencies of the vibrational modes around the IS a and a unitary reduced Planck constant has been considered.

Therefore the probability to be in the basin of attraction of the IS a is

$$p_a(T) = \frac{1}{Z_{\mathrm{IS}}(T)} e^{-\beta [V_a + R_a(T)]}. \tag{14}$$

The free energy of the whole system at equilibrium is simply given by $f_{\mathrm{IS}}(T)=-T \ln[Z_{\mathrm{IS}}(T)]$. However if one is interested to construct a free-energy landscape as a function of a parameter characterizing the different IS, like, e.g., the Kabsch distance δ_K [45] or the end-to-end distance ζ, this is possible by defining a partition function restricted to IS with an end-to-end distance within the narrow interval $[\zeta;\zeta+d\zeta]$,

$$Z_{\mathrm{IS}}(\zeta,T) = \sum_a{}' e^{-\beta [V_a + R_a(T)]}, \tag{15}$$

where the Σ' indicates that the sum is not over the whole ensemble of ISs $\{a\}$ but restricted. The free-energy profile as a function of ζ can be simply obtained by the relationship

$$f_{\mathrm{IS}}(\zeta,T) = -T \ln[Z_{\mathrm{IS}}(\zeta,T)]; \tag{16}$$

while the average potential and free vibrational energy, corresponding to ISs characterized by a certain ζ, can be estimated as follows:

$$V_{\mathrm{IS}}(\zeta,T) = \frac{\sum_a{}' V_a e^{-\beta [V_a + R_a(T)]}}{Z_{\mathrm{IS}}(\zeta,T)},$$

$$R_{\mathrm{IS}}(\zeta,T) = \frac{\sum_a{}' R_a(T) e^{-\beta [V_a + R_a(T)]}}{Z_{\mathrm{IS}}(\zeta,T)}. \tag{17}$$

In order to find the different ISs one can perform MC samplings or molecular dynamics (MD) simulations. We have chosen to examine MD trajectories at constant temperature via a Langevin integration scheme. In particular, we have built up two data banks of ISs: The thermal data bank (TDB) obtained by performing equilibrium canonical simulations and the pulling data bank (PDB) by mechanically unfolding the protein. In order to find the different ISs, the equilibrium (respectively, out-of-equilibrium) Langevin trajectory is sampled at constant time intervals $\delta t=5$ (respectively, at constant elongation increments $\delta\zeta=0.1$) to pinpoint a series of configurations, which afterward are relaxed via a steepest descent dynamics and finally refined by means of a standard Newton's method. In the case of the TDB, in order to speed up the search of ISs we have employed a so-called "quasi-Newton" method [46].[2] For mechanical unfolding, the protein is unblocked and the pulling apparatus removed before the relaxation stage. Two local minima are identified as distinct whenever their energies differ more than 1×10^{-5}. The TDB for the good (respectively, bad) folder contains 579 749 (respectively, 210 782) distinct ISs collected via equilibrium simulations at various temperatures in the range [0.3; 2.0]. The PDB contains 3000–50 000 ISs depending on the examined temperature as detailed in Table II.

V. EXTENDED JARZYNSKI EQUALITY

In the present section, we discuss an extended version of the Jarzynski equality, which allows one to obtain the free-energy profile as a function of a collective coordinate. Let x be the variable that identifies the system microscopic state, e.g., the collection of the positions and momenta of all the

[2]The comparison between the steepest descent and the quasi-Newton methods has revealed that this second minimization scheme is somehow faster (1.8 times faster at $T=0.5$ for the good folder), but while the steepest descent algorithm is able to identify the metastable stationary states in the 99.8% of examined cases the quasi-Newton scheme was successful in the 98.7% of situations. However, the distributions of the identified minima (by considering the same trajectory) obtained with the two schemes are essentially coincident.

TABLE II. Number of distinct ISs contained in the PBD at different temperatures. These have been obtained by sampling, during out-of-equilibrium mechanical unfoldings, several Langevin trajectories at constant elongation increments $\delta\zeta=0.1$. The total number of relaxations performed for each temperature amounts to $\sim$60 000 corresponding to $\sim$200 repetitions of the same pulling experiment. The considered experiments have been performed at $v_P=5\times10^{-4}$ for the *GF*, while velocities in the range $v_P\in[5\times10^{-5}:5\times10^{-4}]$ have been employed for the *BF*. For the bad folder not all temperatures have been examined.

T	Good folder	Bad folder
0.1	2843	456
0.2	5875	1763
0.3	12 359	6477
0.4	35 409	21 060
0.5	52 546	45 950
0.6	51 971	
0.7	54 736	

particles in the system $x=\{\boldsymbol{r}_i,\boldsymbol{p}_i\}$. The system Hamiltonian is a function of x, and will be indicated as $H_0(x)$ in the following. Let $X(x)$ be a macroscopic observable of the system, e.g., the volume, and let us assume that the system is subject to an external potential $U_\lambda(X)$, which is a function of X, and which depends on a parameter λ whose value is externally controlled. The parameter λ changes according to a given time protocol $\lambda(t)$, and thus the system is characterized by a time-dependent Hamiltonian $H(x,t)=H_0(x)+U_{\lambda(t)}(X(x))$. The thermodynamic work done on the system, as the external parameter λ changes, reads as

$$W_t=\int_0^t dt'\dot{\lambda}(t')\,\partial_\lambda U_\lambda(X(x(t')))|_{\lambda=\lambda(t')}. \tag{18}$$

Due to thermal fluctuations, W_t varies between a realization and another one of the manipulation process.

We now introduce the function $f(X,T)$, which is the free energy of the constrained ensemble, in which the value $X(x)$ is fixed at X,

$$f(X,T)=-k_BT\ln\int dx\delta(X-X(x))e^{-\beta H_0(x)}. \tag{19}$$

The extended Jarzynski equality, relates the work done on the system, as an effect of the change in the external parameter λ, with the free energy $f(X,T)$ [23,47,48]

$$Z_0e^{\beta U_{\lambda(t)}(X)}\langle\delta(X-X(x))e^{-\beta W_t}\rangle_t=e^{-\beta f(X,T)}, \tag{20}$$

where $Z_0=\int dx\,\exp[-\beta H_0(x)]$ is the partition function associated with the time-independent Hamiltonian $H_0(x)$ and the averages $\langle\cdots\rangle_t$ are taken over many realizations of the same protocol at time t. Equation (20) provides thus a method to evaluate the unperturbed free energy $f(X,T)$ as long as one has a reliable estimate of the left-hand side (lhs) of this equation. It is worth to note that one does not need to evaluate the partition function Z_0 to evaluate $f(X,T)$, as it appears only as a multiplicative constant in Eq. (20).

The optimal estimate of $f(X,T)$ can be obtained by combining Eq. (20) with the previously discussed method of weighted histograms [23,47,48], namely

$$f_J(X,T)=-k_BT\ln\left(\frac{\sum_t\frac{\langle\delta(X-X(x))\exp(-\beta W_t)\rangle_t}{\langle\exp(-\beta W_t)\rangle_t}}{\sum_t\frac{\exp(-U(X,t))}{\langle\exp(-\beta W_t)\rangle_t}}\right), \tag{21}$$

where the sums Σ_t are over successive time snapshots. For a detailed derivation of Eq. (20) see [47].

VI. THERMODYNAMICAL PROPERTIES

The main thermodynamical features of the examined model can be summarized by reporting three different transition temperatures [1,11,12,49,50]: Namely, the hydrophobic collapse temperature T_θ, the folding temperature T_f, and the glassy temperature T_g.

The collapse temperature discriminates between phases dominated by random-coil configurations rather than collapsed ones [51], T_θ has been usually identified as the temperature where the heat capacity $C(T)$ reaches its maximal value, namely (within the canonical formalism):

$$C(T_\theta)\equiv C^{\max},\quad \text{where } C(T)=\frac{\langle E^2\rangle-\langle E\rangle^2}{T^2}, \tag{22}$$

and $\langle\cdots\rangle$ represents a time average performed over an interval $t\simeq10^5$ by following a US trajectory. From Fig. 2, it is evident that for both sequences $C(T)\sim138$ up to temperatures $T\sim0.25$. This result can be understood by noticing that at low temperatures the thermal features of heteropolymers resemble that of a disordered 3D solid, with an associated heat capacity $C_{\rm sol}\equiv3L$. Moreover, the high-temperature values are smaller than $C_{\rm sol}$, since in this limit we expect that a one-dimensional chain in a three-dimensional space would have a specific heat $C=2L$ [49]. However, as shown in Fig. 2, these extreme temperatures have not yet been reached. The comparison of the heat capacity curves for the *GF* and *BF* reveals that $C(T)$ obtained for the *GF* has a much broader peak with respect to the *BF*. This indicates that the transition from the NC to the random-coil state is definitely sharper for the bad folder.

The folding temperature has been defined in many different ways [31,39,49], however we have chosen to define the folding temperature by employing the IS reconstruction of the phase space. In practice, quite long USs have been performed at various temperatures, up to duration $t=5\,000\,000$. During each of this US the visited ISs have been identified at regular intervals $\delta t=5$, and from these data we have estimated the probability $P_{nc}(T)$ to visit the NC at such temperature (Fig. 3). The folding temperature T_f is then defined as

$$P_{nc}(T_f)\equiv0.5. \tag{23}$$

Indeed, it should be noticed that for the *GF* P_{nc} is the probability to stay in the two lowest-lying energy minima (ISs) and not in the NC only. These two minima can be associated

TABLE III. Transition temperatures estimated for good and bad folder with the corresponding error.

	GF	*BF*
T_θ	0.65(1)	0.46(2)
T_f	0.255(5)	0.24(1)
T_g	0.12(2)	0.27(2)

to a unique attraction basin, since their energy separation is extremely small with respect to $|V_{\mathrm{NC}}|$ (namely, 0.04) and also the corresponding configurations are almost identical, being separated by a Kabsch distance $\delta_K=0.128$. Moreover, at any examined temperature we have always observed a rapid switching between the two configurations, indicating that there is an extremely low-energy barrier among these two states.

The glassy temperature T_g indicates the temperature below which freezing of large conformational rearrangements occurs: Below such a temperature the system can be trapped in local minima of the potential. By following [49], in order to locate T_g we have made a comparison among results obtained from FS and US. In particular, we have examined, at the same temperatures, the average total energy $\langle E\rangle$ of the system evaluated over finite time intervals. As shown, in Fig. 4, these quantities, when obtained from USs and FSs, coincide at temperatures larger than T_g, below which the structural arrest takes place. In particular, unfolding averages have been performed over intervals of duration $t=10^5$ by following a single trajectory. On the other hand, folding simulations have been followed up to times $t\simeq 1.1\times 10^7$ and the averages taken over 5–7 different initial conditions by considering for each trajectory only the last time span of duration $t\simeq 5\times 10^4$. The error bars (standard deviation)

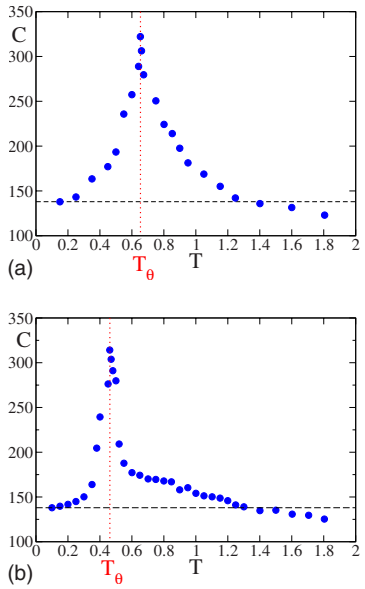

FIG. 2. (Color online) Heat capacity C as a function of the temperature T for good (a) and bad (b) folder; the vertical (red) dotted line indicates the hydrophobic collapse temperature T_θ and the horizontal (black) dashed line the value C_{sol}.

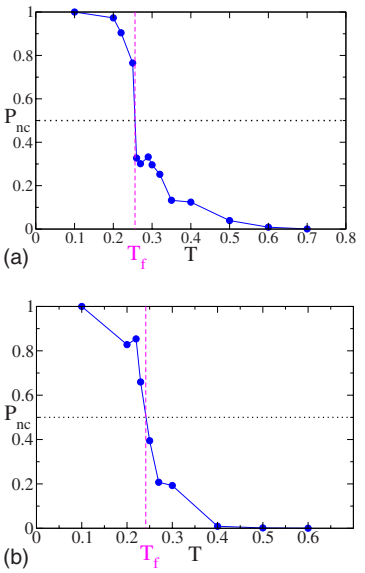

FIG. 3. (Color online) Probability P_{nc} as a function of the temperature T for good (a) and bad (b) folder; the vertical (magenta) dashed line indicates the folding temperature T_f, while the horizontal (black) dotted line refers to the value 0.5.

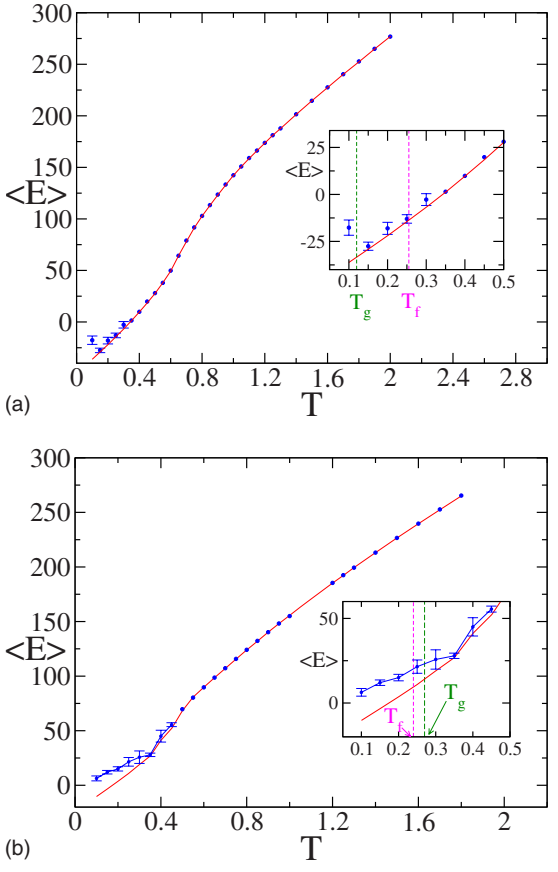

FIG. 4. (Color online) Total energy $\langle E\rangle$ as a function of the temperature T for good (a) and bad (b) folder; the solid (red) line corresponds to US's and the (blue) symbols to FS's. In the inset an enlargement for low temperatures: The dashed lines indicate the glassy (T_g) (magenta) and folding (T_f) (green) temperatures.

shown in Fig. 4 should be interpreted, at sufficiently low temperatures, as a sign of the dependence of the results on the initial conditions.

The three transition temperatures estimated for the good and bad folder are reported in Table III.[3] One can notice that T_θ is larger for the good folder, thus indicating that the collapsed state has a greater stability with respect to the bad folder. Moreover, while for the good folder $T_f > T_g$, for the bad one this order is reversed. Therefore, the *BF* will most likely remain trapped in some misfolded configurations before reaching the NC even at temperatures $T \sim T_f$.

VII. EXTENDED JARZYNSKI EQUALITY RECONSTRUCTION

In this section we present for both the sequences *GF* and *BF* the reconstruction of the FEL, at various temperatures, as a function of the end-to-end distance ζ starting from out-of-equilibrium measurements. The free-energy profiles have been obtained via the EJE by averaging over 28–250 repetitions of the same pulling protocol depending on the pulling velocity as described in Sec. II C. We have generally used the pulling configuration where the first bead is kept fixed and the 46th bead is pulled (tail-pulled case). However, by considering the head-pulled case, where the roles of the first and last bead are reversed. we obtain, for sufficiently low velocities (namely, $v_p \leqslant 5 \times 10^{-4}$ for the *GF* and $v_p \leqslant 5 \times 10^{-5}$ for the *BF*), exactly the same free-energy profile. These results are essentially in agreement with those reported in [42] for the *GF*.

A. Good folder

In Fig. 5(a) are presented the EJE reconstructions $f_J(\zeta)$ (symbols) for $T=0.3$ obtained at various pulling velocities for the good folder together with the corresponding WHAM estimate $f_W(\zeta)$ (dashed lines). As a first point, we notice that the estimated FEL collapses towards $f_W(\zeta)$ as the pulling velocity decreases. In particular, for the good folder the asymptotic shape is reached for small ζ values at a somehow larger velocity (namely, for $\zeta < 10$ already for $v_p = 5 \times 10^{-4}$) than at larger ζ. In particular, to reproduce $f_W(\zeta)$ up to ζ_{trans} the pulling should be performed at $v_p = 5 \times 10^{-6}$. Moreover, referring to Fig. 5, it is possible to identify the structural transitions (STs) induced by the pulling experiment. As shown in Fig. 5(b), the asymptotic $f_J(\zeta)$ profile exhibits a clear minimum in correspondence of the end-to-end distance of the NC (namely, $\zeta_0 \sim 1.9$). In more detail, up to $\zeta \sim 5.6$, the protein remains in nativelike configurations characterized by a β barrel made up of four strands, while the escape from the native valley is signaled by the small dip at $\zeta \sim 5.6$ and it

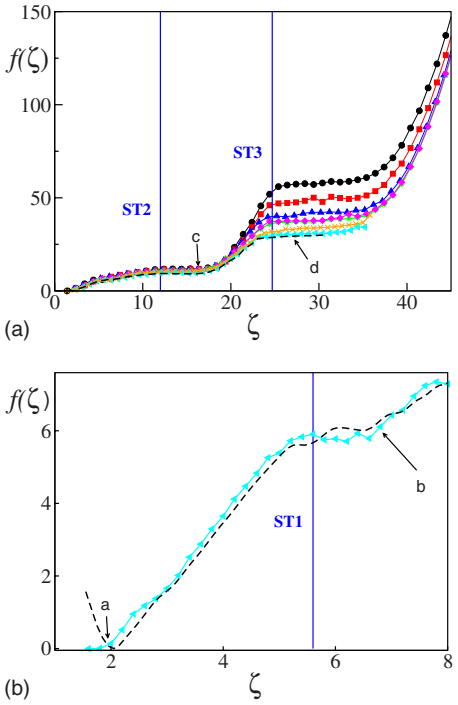

FIG. 5. (Color online) (a) Free-energy profiles f_J for the good folder as a function of the end-to-end distance ζ at $T=0.3$, obtained with the EJE for various pulling velocities: From top to bottom $v_p = 5 \times 10^{-2}$, 1×10^{-2}, 5×10^{-3}, 5×10^{-4}, 2×10^{-4}, 2×10^{-5}, and 5×10^{-6}. In (b) an enlargement of the curve for $v_p = 5 \times 10^{-6}$ at low ζ is reported. The (black) dashed curve in (a) and (b) refers to the WHAM reconstruction $f_W(\zeta)$ with $k_W = 10$. The number of different pulling experiments performed to estimate the profiles ranges between 150 and 250 at the higher velocities to 28 at the lowest velocity $v_p = 5 \times 10^{-6}$. The letters indicate the value of $f(\zeta)$ for the pulled configurations reported in Fig. 6(a) and the (blue) vertical solid lines the location of the STs.

is indicated as ST1 in Fig. 5(b). This ST has been first identified in [41] by analyzing the potential energy of ISs measured during a mechanical unfolding (numerical) experiment. In particular, Lacks [41] identifies this transition as an irreversible transition, in the sense that above this transition it is no more sufficient to reverse the stretching to recover the previously visited configurations.[4]

For $\zeta > 6$ the configurations are characterized by an almost intact core (made of three strands) plus a stretched tail corresponding to the pulled fourth strand [see (b) in Fig. 6(a)]. The second ST amounts to pull the strand $(PB)_5P$ out of the barrel. In the range $13 < \zeta < 18.5$ the curve $f_J(\zeta)$ appears as essentially flat, thus indicating that almost no work is needed to completely stretch the tail once detached from the barrel [see configuration (c) in Fig. 6(a)]. The pulling of the third strand (that is part of the core of the NC) leads to a

[3] In [31] for the sequence *GF* it has been found $T_\theta = 0.65$ and $T_f \sim 0.34$; however in the same paper the authors suggested that the folding transition was associated to a shoulder in the *C*, but this result has been recently criticized [40]. Moreover, more recent estimates, obtained by employing different protocols, suggest that $T_f \sim 0.24$–0.25 [9,11] and $T_g \sim 0.15$ [11], values that are essentially in agreement with our results.

[4] Please notice that we observe this transition at $\zeta \sim 5.6$ and not at $\zeta = 4.782$ as Lacks has reported, since we are considering the free-energy profile at $T=0.3$, while Lacks' analysis concerns potential energies of the ISs. Our inspection of the average potential energies estimated during the pulling experiments and reported in Fig. 14(a) confirms this small mismatch.

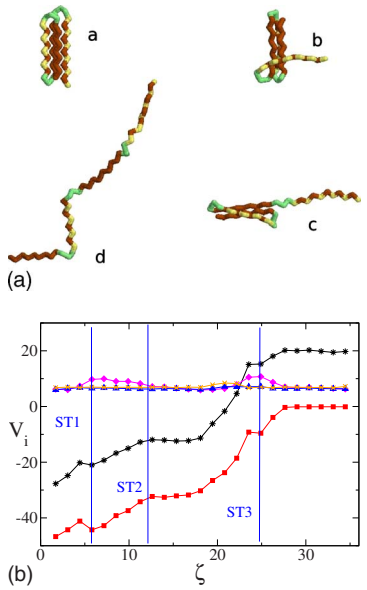

FIG. 6. (Color online) (a) Pulled configurations of the good folder at $T=0.3$: the NC (a) has $\zeta_0 \sim 1.9$; the others are characterized by $\zeta=6.8$ (b), $\zeta=16.8$ (c), and $\zeta=27.1$ (d). The beads of type N, B, and P are colored in green, red and yellow, respectively. (b) Potential energies contributions as a function of the end-to-end distance ζ estimated during a pulling experiment with speed $v_p=5\times10^{-6}$ and obtained by averaging over 28 different realizations at $T=0.3$. (Black) Stars indicate the entire potential energy V, (orange) crosses V_1, (blue) triangles V_2, (magenta) diamonds V_3, and (red) squares V_4. The (blue) vertical solid lines indicate the transitions previously discussed in the text.

definitive destabilization of the β barrel. This transition is denoted as ST3 in Fig. 5(a). The second plateau in $f_J(\zeta)$ corresponds to protein structures made up of a single strand [similar to (d) in Fig. 6(a)].

To distinguish between entropic and energetic costs associated to each ST we have also evaluated separately the potential energy contributions V_i $(i=1,\ldots,4)$ during the pulling experiment, these data are reported in Fig. 6(b). From the figure it is clear that the variation of the potential energy during the stretching is essentially due to the Lennard-Jones term V_4, while the other terms contribute to a much smaller extent, at least up to $\zeta \sim 35$. The transition ST1 has essentially only energetic costs, since $\Delta f=7(1)$ and the potential energy varies almost by the same amount, in particular $\Delta V \sim \Delta V_4=8(1)$. The other transitions instead have no negligible entropic costs, since the free-energy barrier heights associate to ST2 and ST3 are 10(1) and 29(2), respectively; while the corresponding potential energy barriers are higher, namely $\Delta V=16(1)$ for ST2 and $\Delta V=43(1)$ for ST3. The complete stretching of the protein up to $\zeta=35$ has a free (respectively, potential) energy cost corresponding to $\Delta f=30(2)$ [respectively, $\Delta V=49(1)$]. Above $\zeta \sim 35$, while the Lennard-Jones and dihedral contributions vanish, the final (almost quadratic) rise of the free energy is due to the harmonic and angular contributions, since we are now stretching bond distances and angles beyond their equilibrium values. Due to computational constraints and to the fact that this part of the FEL is not particularly relevant, the reconstructions at

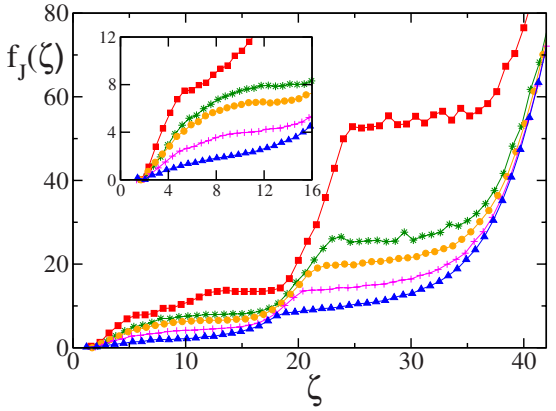

FIG. 7. (Color online) Free-energy profiles $f_J(\zeta)$ obtained with the EJE for good folder at various temperatures: $T=0.2$ (red squares), 0.4 (green stars), 0.5 (orange circles), 0.6 (magenta plus), and 0.7 (blue triangles). In the inset, an enlargement is reported at small ζ. Data refer to $v_p=5\times10^{-4}$. The number of different realizations performed to estimate the averages at the different temperatures ranges between 160 and 250.

the lowest velocities and the WHAM estimations have been not performed for these large ζ values.

In Fig. 7 the reconstruction of the FEL obtained at various temperatures is shown. For temperatures around T_f one still observes a FEL resembling the one found for $T=0.3$, while by increasing the temperature the dip around $\zeta \sim 6-7$ (associated to ST1) disappears and the heights of the other two barriers reduce. By approaching T_θ the first plateau, characterizing the transition from the NC to configurations of type (c), essentially disappears, and it is substituted by a monotonous increase of $f_J(\zeta)$. This suggests that four stranded β-barrel configurations coexist with partially unfolded ones. Above T_θ only one barrier remains indicating that at these temperatures the protein unfolds completely in a one-step process.

The connection between dynamical properties of the system and the free-energy profile is still an open problem. In particular, the relationship between the unfolding times and the free-energy barriers has been previously discussed in Ref. [52] for proteins and more recently the same problem has been addressed for the Ising-like lattice protein model in Ref. [53]. We have estimated average first passage times τ via USs by recording the time needed for the protein to reach a certain end-to-end threshold $\zeta_{\rm th}$ once it starts from the NC at different temperatures. Our data, reported in Fig. 8, clearly indicate that at low temperatures the simple result of the transition state theory [54–56], namely

$$\tau = \frac{e^{\Delta f/T}}{T}, \tag{24}$$

where $\Delta f=f(\zeta_{\rm th})-f(\zeta_0)$, is in very good agreement with the numerics. However, at high temperatures the agreement worsens. Therefore, in order to take in account all of the details of the free-energy profile and not only the barrier height, we have generalized a result of the Smoluchowski

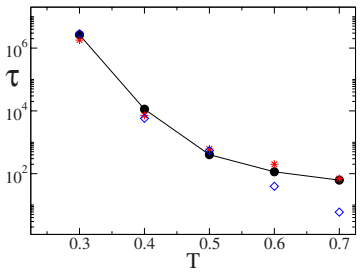

FIG. 8. (Color online) Average unfolding times τ for the *GF* at various temperatures corresponding to $\zeta_{\text{th}}=4$. Filled (black) circles denote the numerical data, the estimations obtained via Eq. (24) and Eq. (25) are represented by empty (blue) diamonds and (red) stars, respectively. The arbitrary scaling factor entering in Eq. (25) (see text) has been set equal to 8. The average times have been estimated over 100 000–200 000 unfolding events for $T=0.7$ and 0.6, 12 000 events at $T=0.5$ and as few as 200 and 60 events at the lowest temperatures, namely $T=0.4$ and 0.3.

theory for the escape of a particle from a potential well [56] as follows [53]:

$$\tau \propto \frac{1}{T}\int_{\zeta_0}^{\zeta_{\text{th}}} dy e^{f(y)/T}\int_{\zeta_0}^{y} dz e^{-f(z)/T}, \tag{25}$$

where the potential energy has been substituted by the free-energy profile. The estimation obtained via Eq. (25) compare well with the numerical results at all of the considered temperatures, unfortunately apart from an arbitrary scaling factor common to all of the temperatures that we are unable to estimate (see Fig. 8).

B. Bad folder

In Fig. 9(a) are reported the free-energy profiles $f_J(\zeta)$ reconstructed via the EJE at $T=0.3$ for different pulling speeds (symbols) together with the estimated $f_W(\zeta)$ (dashed line), as in the case of the *GF* one observes a collapse to the equilibrium FEL [represented by $f_W(\zeta)$] for a sufficiently small speed. In particular, at $v_p=5\times10^{-6}$ a reasonably good agreement between f_J and f_W is already achieved.

For the *BF* the mechanically induced unfolding transitions are less clearly identifiable from the inspection of the free-energy profile for two reasons. First, for the *BF* not only the LJ interactions play a role in the STs but also the dihedral terms: These two terms contribute with opposite signs to the whole potential energy thus partially canceling each other. Moreover, as we will show in the following the main contribution to the free energy is due to entropic terms. Therefore, in order to identify the STs it is better to consider the distinct average profile of the single potential contributions V_i $(i=1,\ldots,4)$ reported in Fig. 9(b). In particular, the most relevant is the Lennard-Jones term V_4, due to the stabilizing effect of the hydrophobic interactions on the protein structure. From the inspection of V_4, at least four different STs can be singled out, occurring at $\zeta\sim7.3$, 14.5, 19.3, and 26.3, respectively.

The first transition amounts to pull the last part of the tail out of the NC, namely the sixth and fifth strand that we have

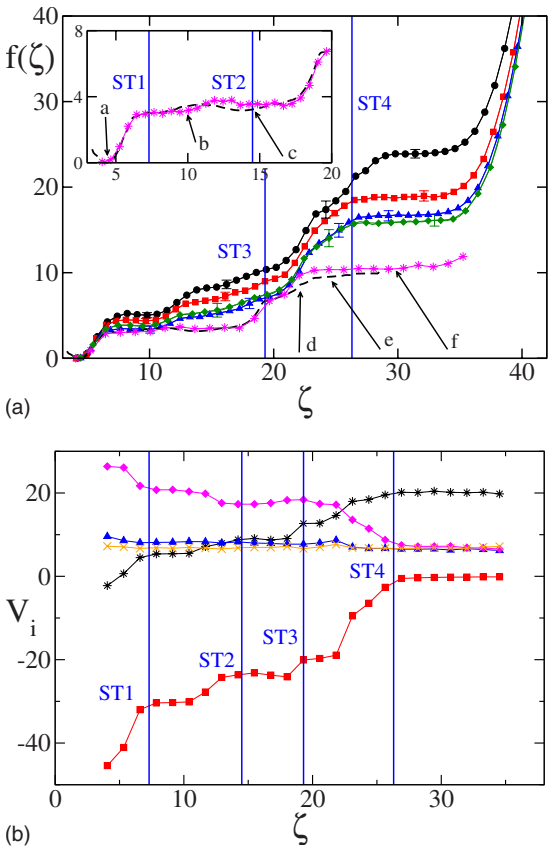

FIG. 9. (Color online) (a) Free-energy profiles f_J for the bad folder as a function of the end-to-end distance ζ, obtained with the EJE for various pulling velocities: From top to bottom $v_p=5\times10^{-4}$ and 160 realizations (black circles), 2×10^{-4} and 200 realizations (red squares), 1×10^{-4} and 200 realizations (blue triangles), 5×10^{-5} and 100 realizations (green diamonds), 5×10^{-6} and 28 realizations (magenta stars). The WHAM estimate $f_W(\zeta)$ is also shown (black dashed line). In the inset an enlargement of the curve at low ζ for $v_p=5\times10^{-6}$ is reported together with $f_W(\zeta)$. Data have been obtained at $T=0.3$. (b) Potential energies contribution as a function of the end-to-end distance ζ estimated during a pulling experiment with velocity $v_p=5\times10^{-6}$ and obtained by averaging over 28 different realizations at $T=0.3$. Black stars indicate the entire potential energy V, (orange) crosses V_1, (blue) triangles V_2, (magenta) diamonds V_3, and (red) squares V_4. The (blue) solid lines indicate the transitions discussed in the text.

previously identified. To this ST is associated a free energy increase of 3.1(5) and a potential energy variation of 8.0(5), once the ST1 is completed the protein assumes the configuration (b) shown in Fig. 10. ST2 consists in pulling out from the compact configuration the whole tail (therefore to detach also the fourth strand) and leaving the protein in a configuration composed by the core (represented by the first three strands) plus a long tail [see configuration (c) in Fig. 10]. The entropic contributions to ST2 is quite relevant since to pass from the NC to (c) the free energy increases of 3.8(5), while the associated potential energy variation is almost the triple, i.e., 11.5(5). The third transition amounts to detach the first β strand ($BNBPB_3NP$) from the core and this operation has much greater costs with respect to the previous STs, namely, $\Delta f=7.0(5)$ and $\Delta V=15(1)$. The complete opening of

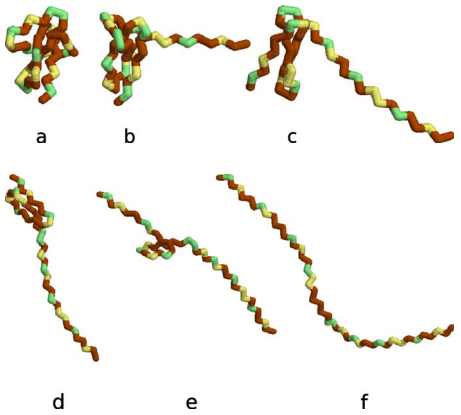

FIG. 10. (Color online) Pulled configurations of the bad folder at $T=0.3$: The reported configurations refer to $\zeta_0=4.7$ (NC) (a), $\zeta=9.9$ (b), 14.5 (c), 22.1 (d), 24.6 (e), and 29.7 (f).

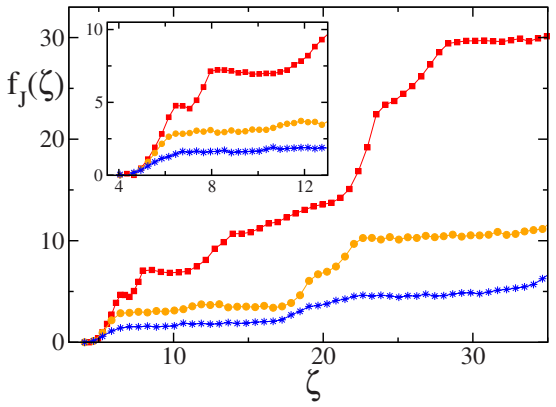

FIG. 11. (Color online) Free-energy profiles $f_J(\zeta)$ obtained via the EJE for bad folder at three temperatures: Namely, $T=0.2$ (red squares), $T=0.3$ (orange circles), $T=0.4$ (blue stars). In the inset an enlargement is reported at small ζ. Data refer to pulling velocity $v_p=5\times10^{-6}$ and the averages are performed over 28 samples of the same protocol.

the core structure (now made only of the second and third strand) occurs at $\zeta\sim27$ amounting to a total free (respectively, potential) energy barrier to overcome the height 11(1) [respectively, 23(1)]. At variance with the *GF* case, for the *BF* the entropic costs are never negligible and instead they always amount to at least one-half of the potential energy contributions in all four examined transitions. Finally, analogously to the *GF* for $\zeta>35$ the LJ and dihedral contributions essentially vanish and the free energy increase is due to the harmonic and angular terms, only.

In Fig. 11 the reconstruction f_J of the FEL for the bad folder is reported at three temperatures below T_θ. As one can notice the bad folder exhibits at comparable temperatures much lower free-energy barriers, indicating that the NC and the partially folded structures are less stable, with respect to the *GF*. This is reflected also in the value of T_θ that has a smaller value with respect to the *GF*: Namely, 0.46 for *BF* and 0.65 for *GF*. By increasing T the heights of the free-energy barriers rapidly decrease and the various STs become less clearly defined. Moreover, the FEL of the *BF* at the lower examined temperature ($T=0.2$) reveals, besides the absolute minimum (corresponding to the NC), other two local minima at $\zeta\sim7$ and $\zeta\sim11$. This indicates that, at variance with the *GF*, the *BF* can remain trapped even at $T\sim T_f$, for some finite time, in intermediate (misfolded) states far from the NC.

VIII. INHERENT STRUCTURE LANDSCAPE

In this section we compare the reconstructions of the FEL for the good and bad folder obtained via the EJE and the IS approach with the WHAM equilibrium estimation. As already explained in Sec. IV, we have created two IS data banks: The thermal data bank (TDB) obtained by performing equilibrium canonical simulations and the pulling data bank (PDB) by mechanically unfolding the protein. Figure 12 reports the *GF* comparison, at three temperatures, between the estimate $f_W(\zeta)$ with $f_{\rm IS}(\zeta)$ and the $f_J(\zeta)$, obtained via the EJE reconstruction. The results reveal an astonishingly good coincidence between $f_W(\zeta)$ and $f_{\rm IS}(\zeta)$, obtained by employing the PDB, at all the examined temperatures. For what concerns the EJE reconstructions: At $T=0.3$ $f_J(\zeta)$ is essentially in good agreement with the other two estimations, while at higher temperatures the f_J curves slightly overestimate the equilibrium free energy f_W for $\zeta>10$. This discrepancy is probably due to a noncomplete convergence of the EJE approach at the considered pulling velocities, smaller velocities are required to recover the equilibrium profile at all the end-to-end distances.

The further comparison reported in Fig. 12 between the IS reconstructions obtained via the TDB and the PDB indicates a perfect coincidence up to $\zeta\sim17$. On the contrary, during the last stage of the unfolding process the two $f_{\rm IS}$ differ: The TDB FEL is steeper than the PDB one. This suggests that during the mechanical unfolding the protein can easier reach states with low energies, even at large ζ. These states have a very low probability to be visited during thermal equilibrium dynamics. However, at $T=0.3$ the value of the barrier to overcome and that of the final plateau are quite similar to those of the PDB FEL, while at higher temperatures the final

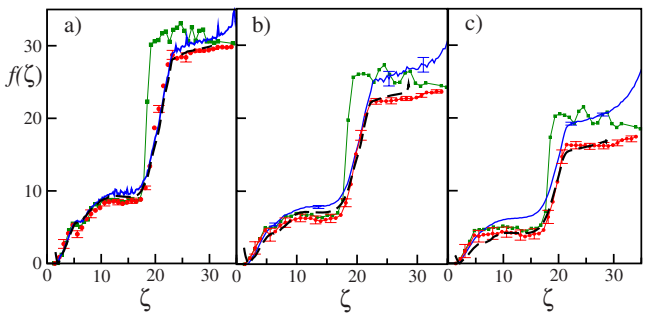

FIG. 12. (Color online) Free-energy profiles f_J (blue solid lines) as a function of ζ for various temperatures for the good folder: (a) $T=0.3$ for $v_p=5\times10^{-6}$ and 28 repetitions; (b) $T=0.4$ for $v_p=5\times10^{-4}$ and 240 experiments; (c) $T=0.5$ for $v_p=5\times10^{-4}$ and 240 repetitions. The (black) dashed lines refer to the WHAM estimation $f_W(\zeta)$, (green) squares to $f_{\rm IS}(\zeta)$ obtained by employing the TDB and (red) circles to $f_{\rm IS}(\zeta)$ obtained by employing the ISs in the PDB for each considered T.

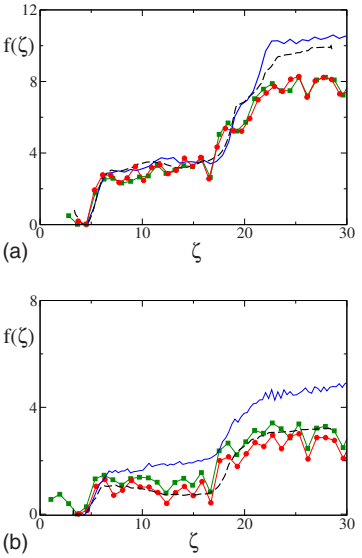

FIG. 13. (Color online) Free-energy profiles f_J as a function of ζ for various temperatures for the bad folder: (a) $T=0.3$ and (b) $T=0.4$. The data refer to a pulling velocity $v_P=5\times10^{-6}$ and 28 repetitions of the same pulling protocol. The symbols are the same as in Fig. 12.

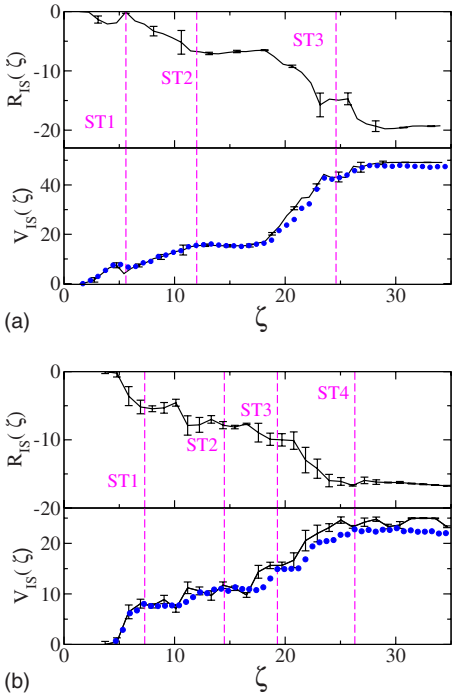

FIG. 14. (Color online) Reconstructed $V_{IS}(\zeta)$ (lower panel) and $R_{IS}(\zeta)$ (upper panel) for good folder (a) and bad folder (b) by employing ISs in the PDB at $T=0.3$. In the lower panel the blue dotted line refers to the average potential energy evaluated during the corresponding pulling experiments [this has been already reported in Fig. 6(b) for the *GF* and in Fig. 9(b)] for the *BF*. Please notice that the data have been vertically translated in order to have zero energy at the NC.

energy plateaus of the TDB FEL are slightly larger than the f_W plateaus. The reason for these discrepancies is related to the fact that, despite the high number of IS forming the TDB, this data bank is far from containing all the relevant ISs, in particular those associated to high ζ values are lacking. It should be remarked that the IS conformation with the maximal end-to-end distance is the all *trans*-configuration, corresponding to $\zeta_{trans}=35.70$, therefore the IS approach does not allow us to evaluate the FEL for $\zeta>\zeta_{trans}$. For the *GF*, we can safely affirm that the out-of-equilibrium process consisting in stretching the protein is more efficient to investigate the FEL, since a much smaller number of ISs are needed to reliably reconstruct it, as reported in Table II.

The comparison for the *BF* case is reported in Fig. 13 at $T=0.3$ and 0.4. Also in this case the $f_W(\zeta)$ and $f_{IS}(\zeta)$ essentially coincide, apart at $T=0.3$ and $\zeta>20$ where f_W is slighty higher than f_{IS}. In this case the agreement between the two IS reconstructions is quite good at both the considered temperatures and for all ζ values. As far as the EJE reconstructions are concerned, at the employed pulling velocity (namely, $v_P=5\times10^{-6}$) f_J can be considered as asymptotic at $T=0.3$, while probably at $T=0.4$ is still slightly overestimating f_W, but notice the really small range of the free-energy scale reported in Fig. 13(b) with respect to the *GF*.

Furthermore, from the IS analysis by employing Eq. (17) we can obtain an estimate of the profiles of the potential and vibrational free energies $V_{IS}(\zeta)$ and $R_{IS}(\zeta)$, respectively. From the latter quantity, the entropic costs associated to the various unfolding stages can be estimated. As shown in Fig. 14(a), for the *GF* at $T=0.3$, the structural transitions ST2 and ST3 previously described correspond to clear "entropic" barriers, while the ST1 transition has only energetic costs since $\Delta R_{IS}\sim0$. This last result is in good agreement with the previously reported EJE analysis. For what concerns the other two transitions, ST2 (respectively, ST3) is associated to a decrease $\sim6(1)$ [respectively, 15(2)] of $R_{IS}(\zeta)$ once more in agreement with the EJE reconstruction. The complete opening of the protein is associated to a barrier $\Delta R_{IS}(\zeta)=20(2)$, while the analysis reported in Sec. VII A indicates an entropic barrier to overcome corresponding to $\sim19(2)$. These results suggest that for the good folder the entropic contributions to the free energy are essentially of the vibrational type. Moreover, the reconstructed potential energies $V_{IS}(\zeta)$ are in very good agreement with the average potential energy evaluated during the corresponding pulling experiments as shown in Fig. 14(a).

Finally, one can try to put in correspondence the three unfolding stages previously discussed for the *GF* with thermodynamical aspects of the protein folding. In particular, by considering the energy profile $V_{IS}(\zeta)$, an energy barrier ΔV_{IS} and a typical transition temperature $T_t=(2\Delta V_{IS})/(3N)$ can be associated to each of the STs. The first transition ST1 corresponds to a barrier to overcome $\Delta V_{IS}=8(1)$ and therefore to $T_t=0.11(1)$, that, within error bars, coincide with T_g. For the ST2 transition the barrier to overcome is $\Delta V_{IS}=16(1)$ and this is associated to a temperature $T_t\simeq0.23(2)$ (slightly smaller than T_f). At the ST3 transition $\Delta V_{IS}=43(2)$ corresponding to $T_t=0.62(2)$, while the energetic cost to completely stretch the protein is 50(2) with an associated transition temperature $T_t=0.72(2)$: The θ temperature [$T_\theta=0.65(1)$] is well bracketed within these two transition temperatures. At least for the *GF*, our results indicate that the

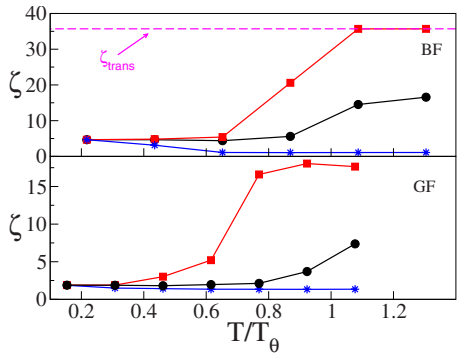

FIG. 15. (Color online) End-to-end distance of the ISs estimated during USs at various temperatures: (Black) Circles represent the average value; (blue) stars the minimal value; and (red) squares the maximal one. The upper panel refers to the *BF* and the lower one to the *GF*. The horizontal magenta dashed line indicates the ζ_{trans} value. For the *GF* (respectively, *BF*) trajectories of duration $t \sim 100\,000-500\,000$ (respectively, $t \sim 50\,000-250\,000$) have been examined to obtain the ISs at constant time intervals $\Delta t=5$.

observed STs induced by pulling can be put in direct relationship with the thermal transitions usually identified for the folding-unfolding process.

Also for the *BF* the IS approach is able to well reproduce not only the average potential energy during the pulling experiment, as clearly shown in Fig. 14(b), but also to provide a good estimate of the "entropic" barriers associated to the structural transitions. In particular, at $T=0.3$ the vibrational free-energy barriers to overcome are $\Delta R_{IS}=5.3(5)$ at ST1, 8(1) at ST2, 10(1) at ST3 and 16(1) at ST4. These values are in reasonably good agreement with those previously obtained from the EJE reconstruction, apart from ST3 and ST4, where the analysis performed in Sec. VII B indicates entropic barriers to overcome corresponding to ~8(1) and ~12(2), respectively. These underestimations at large ζ values are probably due to the fact that at this temperature the estimated f_J has not reached its asymptotic shape at the employed velocity.

As already previously pointed out, the entropic contributions for the *BF* are more relevant than for the *GF*: e.g., while the ST2 transition is clearly visible by the potential energy inspection it is almost absent by looking to the free-energy profile [compare the data reported Figs. 9(a) and 9(b)]. Therefore, we cannot expect to infer information on the thermal transitions from the knowledge of the potential energy barriers at the STs, as done for the *GF*. Indeed the estimated transition temperatures T_t for the four examined structural transitions give values not corresponding to any of the relevant temperatures reported in Table III for the *BF*.

To better understand this difference we have performed USs for the *GF* and *BF* for $T_g \lesssim T \lesssim T_\theta$ and we have estimated the average, the minimal and the maximal ζ associated to the visited ISs. The corresponding data are reported in Fig. 15. While for the *GF* the minimal value remains essentially ζ_0 for all the temperatures and the maximum ζ increases smoothly up to ~18 at $T=T_\theta$, the dependence of the minimal and maximal ζ values on T are more dramatic for the *BF*. Up to the temperatures $T \sim 0.5 \times T_\theta$, average, minimal and maximal ζ values almost coincide indicating that the protein is still confined around the NC, please remember that for the *BF* $T_g=0.58 \times T_\theta$. As soon as $T>0.6 \times T_\theta$ the maximum grows abruptly and reach the upper bound corresponding to ζ_{trans} already at $T \sim T_\theta$, on the other hand, the minimum value decreases indicating that at higher temperatures the protein can access basins of ISs with end-to-end distance lower than ζ_0. This last result indicates that there is not a clear monotonic correspondence between the temperature increase and the achievable protein extensions. Moreover, the fact that the protein can easily attain also extremely stretched configurations at not too high temperatures suggests that in the case of the *BF* the protein can easily escape from the native valley and reach any part of the phase space, while for the *GF* the accessible IS configurations are much more limited at comparable temperatures. All this amounts to say that the end-to-end distance cannot be considered as a good reaction coordinate for the *BF*.

IX. CONCLUDING REMARKS

In conclusion, we can safely affirm that the reconstructions of the free-energy landscape as a function of the end-to-end distance in terms of the ISs, obtained via out-of-equilibrium mechanical unfolding of the heteropolymers, are in very good agreement with the equilibrium weighted histogram estimate for the good and bad folder sequences at all of the examined temperatures. In particular, this result indicates that the harmonic approximation employed to estimate the vibrational term (13) is quite good for temperatures in the range $[T_f;T_\theta]$, as already pointed out in [11] by considering the average potential energy. Moreover, the EJE reconstructions of the free-energy profile compare quite well with the other two approaches for sufficiently low pulling velocities. For the good folder, the quality of the free-energy landscape reconstruction via the extended Jarzinsky equality can be well appreciated by stressing that from pure structural information about the landscape a good estimate of dynamical quantities, like the unfolding times from the native configuration, can be obtained.

Furthermore, for the good folder the information obtained by the equilibrium FEL both with the EJE and the IS methodologies can be usefully combined to give substantiated hints about the thermal unfolding. In particular the investigation of the ISs allows us to give an estimate of the (free) energetic and entropic barriers separating the native state from the completely stretched configuration. These barriers are associated to the structural transition induced by the protein manipulation and for the good folder they can put in direct relationship with the thermal transitions usually identified during folding-unfolding processes.

On the other hand, for the bad folder the end-to-end distance appears not to represent a good reaction coordinate, since mechanical and thermal unfolding seem to follow different paths. In other terms the unfolding process for the good folder consists of many small successive rearrangements of the NC, which are well captured by the distribution of the corresponding ISs on the landscape. While for the bad folder the thermal unfolding can involve also large conformational rearrangements, thus implying jumps from one val-

ley to another of the landscape associated to large variations in the end-to-end distance, that cannot be well reproduced by the mechanical stretching of the heteropolymer. Future work on more realistic heteropolymer models is needed to clarify if the observed features, distinguishing good folders from bad folders, can be really considered as a specific trademark of proteins.

A drawback of the EJE reconstruction is that extremely small velocities or an extremely large number of repetitions of the protocol are needed to achieve the collapse towards the equilibrium profile, thus rendering the implementation of the method quite time consuming. However, new optimized methods to obtain the asymptotic FEL, by combining the Jarzinsky equality with the Crooks' path ensemble average theorem, have been recently presented [57,58] and it will be definitely worth testing their performances in the future with respect to complex landscapes, like those of heteropolymers [59].

As a final point, we would like to remember that, in the context of glassy systems, the concept of ISs has been critically compared to that of pure states [60], the latter being local minima of the free-energy landscape, while the ISs are minima of the potential energy, as discussed above. The relevance of the pure states for protein folding has been recently stressed in Ref. [61], where it has been shown for a fibronectin domain that pure states can be put in direct correspondence with unfolding intermediates observable during mechanical pulling. However, in the present paper we have been only interested in how the FEL, which is the only thermodynamical relevant function, together with the corresponding pure states, can be obtained by employing a suitably chosen ensemble of ISs.

ACKNOWLEDGMENTS

Useful discussions are acknowledged with L. Bongini, L. Casetti, L. Delfini, S. Lepri, R. Lima, R. Livi, L. Peliti, A. Politi, A. Rampioni, F. Sbrana, L. Tsimiring, and M. Vassalli. In particular, we are in debt with R. Chelli and P. Procacci for a critical reading of our results and for fruitful continuous interactions. Moreover, the field potential here employed has been developed by A. Rampioni in collaboration with L. Bongini, R. Livi, A. Politi and one of the authors (A.T.). We acknowledge CINECA in Bologna and INFM for providing us access to the Beowulf Linux cluster under the Grant Iniziativa Calcolo Parallelo. This work has been partially supported by the European Community via the STREP project EMBIO NEST Contract No. 12835.

[1] D. J. Wales, *Energy Landscapes* (Cambridge University Press, Cambridge, 2003).
[2] F. H. Stillinger and T. A. Weber, Science **225**, 983 (1984).
[3] S. Sastry, P. G. Debenedetti, and F. H. Stillinger, Nature (London) **393**, 554 (1998).
[4] L. Angelani, R. Di Leonardo, G. Ruocco, A. Scala, and F. Sciortino, Phys. Rev. Lett. **85**, 5356 (2000).
[5] T. S. Grigera, A. Cavagna, I. Giardina, and G. Parisi, Phys. Rev. Lett. **88**, 055502 (2002).
[6] Z. Guo and D. Thirumalai, J. Mol. Biol. **263**, 323 (1996).
[7] M. A. Miller and D. J. Wales, J. Chem. Phys. **111**, 6610 (1999); P. N. Mortenson and D. J. Wales, *ibid.* **114**, 6443 (2001); P. N. Mortenson, D. A. Evans, and D. J. Wales, *ibid.* **117**, 1363 (2002).
[8] S. V. Krivov and M. Karplus, J. Chem. Phys. **117**, 10894 (2002).
[9] D. A. Evans and D. J. Wales, J. Chem. Phys. **118**, 3891 (2003).
[10] N. Nakagawa and M. Peyrard, Proc. Natl. Acad. Sci. U.S.A. **103**, 5279 (2006); Phys. Rev. E **74**, 041916 (2006).
[11] J. Kim and T. Keyes, J. Phys. Chem. B **111**, 2647 (2007).
[12] A. Baumketner, J.-E. Shea, and Y. Hiwatari, Phys. Rev. E **67**, 011912 (2003).
[13] D. A. Evans and D. J. Wales, J. Chem. Phys. **121**, 1080 (2004).
[14] P. E. Leopold, M. Montal, and J. N. Onuchic, Proc. Natl. Acad. Sci. U.S.A. **89**, 8721 (1992).
[15] M. Carrion-Vazquez *et al.*, Proc. Natl. Acad. Sci. U.S.A. **96**, 3694 (1999); B. Onoa *et al.*, Science **299** 1892 (2003).
[16] M. Carrion-Vazquez *et al.*, Nat. Struct. Biol. **10**, 738 (2003).
[17] A. Irbäck, S. Mitternacht, and S. Mohanty, Proc. Natl. Acad. Sci. U.S.A. **102**, 13427 (2005).
[18] D. J. Brockwell, *et al.*, Nat. Struct. Biol. **10**, 731 (2003).
[19] A. Imparato and L. Peliti, Eur. Phys. J. B **39**, 357 (2004).
[20] C. Jarzynski, Phys. Rev. Lett. **78**, 2690 (1997); G. E. Crooks, Phys. Rev. E **60** 2721 (1999).
[21] D. Collin *et al.*, Nature (London) **437**, 231 (2005).
[22] D. K. West, P. O. Olmsted, and E. Paci, J. Chem. Phys. **125**, 204910 (2006).
[23] G. Hummer and A. Szabo, Proc. Natl. Acad. Sci. U.S.A. **98**, 3658 (2001).
[24] T. Speck and U. Seifert, Phys. Rev. E **70**, 066112 (2004).
[25] A. Imparato and L. Peliti, Europhys. Lett. **70**, 740 (2005).
[26] A. Imparato and L. Peliti, Phys. Rev. E **72**, 046114 (2005).
[27] N. C. Harris, Y. Song, and C.-H. Kiang, Phys. Rev. Lett. **99**, 068101 (2007).
[28] A. Imparato, F. Sbrana, and M. Vassalli, Europhys. Lett. **82**, 58006 (2008).
[29] A. Imparato, S. Luccioli, and A. Torcini, Phys. Rev. Lett. **99**, 168101 (2007).
[30] Z. Guo and D. Thirumalai, Biopolymers **36**, 83 (1995).
[31] Z. Guo and C. L. Brooks III, Biopolymers **42**, 745 (1997).
[32] S. Fowler *et al.*, J. Mol. Biol. **322**, 841 (2002).
[33] E. Paci and M. Karplus, Proc. Natl. Acad. Sci. U.S.A. **97**, 6521 (2000).
[34] D. K. West, P. O. Olmsted, and E. Paci, J. Chem. Phys. **124**, 144909 (2004).
[35] G. M. Torrie and J. P. Valleau, Chem. Phys. Lett. **28**, 578 (1974).
[36] A. M. Ferrenberg and R. H. Swendsen, Phys. Rev. Lett. **63**, 1195 (1989); S. Kumar *et al.*, J. Comput. Chem. **13**, 1011 (1992); B. Roux, Comput. Phys. Commun. **91**, 275 (1995).
[37] J. D. Honeycutt and D. Thirumalai, Proc. Natl. Acad. Sci.

U.S.A. **87**, 3526 (1990).
[38] R. S. Berry, N. Elmaci, J. P. Rose, and B. Vekhter, Proc. Natl. Acad. Sci. U.S.A. **94**, 9520 (1997).
[39] T. Veitshans, D. Klimov, and D. Thirumalai, Folding Des. **2**, 1 (1997).
[40] J. G. Kim, J. E. Straub, and T. Keyes, Phys. Rev. Lett. **97**, 050601 (2006).
[41] D. J. Lacks, Biophys. J. **88**, 3494 (2005).
[42] F.-Y. Li, J.-M. Yuan, and C.-Y. Mou, Phys. Rev. E **63**, 021905 (2001).
[43] A. Blondel and M. Karplus, J. Comput. Chem. **17**, 1132 (1996).
[44] A. Rampioni, Ph.D. thesis, Firenze, 2005.
[45] W. Kabsch, Acta Crystallogr., Sect. A: Cryst. Phys., Diffr., Theor. Gen. Crystallogr. **A32**, 922 (1976).
[46] W. H. Press *et al.*, *Numerical Recipes* (Cambridge University Press, New York, 1994).
[47] A. Imparato and L. Peliti, J. Stat. Mech.: Theory Exp. (2006) P03005.
[48] O. Braun, A. Hanke, and U. Seifert, Phys. Rev. Lett. **93**, 158105 (2004).
[49] A. Torcini, R. Livi, and A. Politi, J. Biol. Phys. **27**, 181 (2001).
[50] L. Bongini, R. Livi, A. Politi, and A. Torcini, Phys. Rev. E **68**, 061111 (2003); **72**, 051929 (2005).
[51] P-G De Gennes, *Scaling Concepts in Polymer Physics* (Cornell University Press, New York, 1979).
[52] D. K. West, E. Paci, and P. D. Olmsted, Phys. Rev. E **74**, 061912 (2006).
[53] A. Imparato, A. Pelizzola, and M. Zamparo, Phys. Rev. Lett. **98**, 148102 (2007).
[54] J. S. Langer, Ann. Phys. **54**, 258 (1969).
[55] P. Hänggi, P. Talkner, and M. Borkovec, Rev. Mod. Phys. **62**, 251 (1990).
[56] R. Zwanzig, *Nonequilibrium Statistical Mechanics*, (Oxford University Press, Oxford, 2001).
[57] R. Chelli, S. Marsili, and P. Procacci, Phys. Rev. E **77**, 031104 (2008).
[58] D. D. L. Minh and A. B. Adib, Phys. Rev. Lett. **100**, 180602 (2008).
[59] R. Chelli, A. Imparato, S. Luccioli, P. Procacci, and A. Torcini (unpublished).
[60] G. Biroli and R. Monasson, Europhys. Lett. **50**, 155 (2000).
[61] S. Mitternacht, S. Luccioli, A. Torcini, A. Imparato, and A. Irbäck (unpublished).